



## LJMU Research Online

**Shanbara, HK, Ruddock, F and Atherton, W**

**Predicting the rutting behaviour of natural fibre-reinforced cold mix asphalt using the finite element method**

<http://researchonline.ljmu.ac.uk/id/eprint/8593/>

### Article

**Citation** (please note it is advisable to refer to the publisher's version if you intend to cite from this work)

**Shanbara, HK, Ruddock, F and Atherton, W (2018) Predicting the rutting behaviour of natural fibre-reinforced cold mix asphalt using the finite element method. Construction and Building Materials, 167. pp. 907-917. ISSN 0950-0618**

LJMU has developed **LJMU Research Online** for users to access the research output of the University more effectively. Copyright © and Moral Rights for the papers on this site are retained by the individual authors and/or other copyright owners. Users may download and/or print one copy of any article(s) in LJMU Research Online to facilitate their private study or for non-commercial research. You may not engage in further distribution of the material or use it for any profit-making activities or any commercial gain.

The version presented here may differ from the published version or from the version of the record. Please see the repository URL above for details on accessing the published version and note that access may require a subscription.

For more information please contact [researchonline@ljmu.ac.uk](mailto:researchonline@ljmu.ac.uk)

<http://researchonline.ljmu.ac.uk/>

1 **Predicting the rutting behaviour of natural fibre-reinforced cold**  
2 **mix asphalt using the finite element method**

3 **Hayder Kamil Shanbara<sup>a,c,\*</sup>, Felicite Ruddock<sup>b</sup> and William Atherton<sup>b</sup>**

4 <sup>a</sup> Department of Civil Engineering, Faculty of Engineering and Technology, Liverpool John Moores University,  
5 Henry Cotton Building, Liverpool L3 2ET, UK

6 <sup>b</sup> Department of Civil Engineering, Faculty of Engineering and Technology, Liverpool John Moores University,  
7 Peter Jost Centre, Liverpool L3 3AF, UK

8 <sup>c</sup> Civil Engineering Department, College of Engineering, Al Muthanna University, Sammawa, Iraq

9 \*Corresponding author

10 E-mail address: [H.K.Shanbara@2014.ljmu.ac.uk](mailto:H.K.Shanbara@2014.ljmu.ac.uk), [hayder.shanbara82@gmail.com](mailto:hayder.shanbara82@gmail.com)

11

12 **Abstract:**

13 This paper describes the development of a three-dimensional (3-D), finite element model  
14 (FEM) of flexible pavements made with cold mix asphalt (CMA), which has itself been  
15 reinforced with two different natural fibres: jute and coir. A 3-D finite element model was  
16 employed to predict the viscoelastic response of flexible CMA pavements when subjected to  
17 multiple axle loads, different bituminous material properties, tire speeds and temperatures. The  
18 analysis was conducted by the finite element computer package ABAQUS/STANDARD. The  
19 pavements were subject to cyclic and static loading conditions to test for permanent  
20 deformation (rutting). The accuracy of the developed model was validated by comparing the  
21 predicted results with those measured in the lab. Reinforced and unreinforced CMA mixture  
22 models were simulated in this research. The results indicate that the CMA mixtures reinforced  
23 with natural fibres, are effective in mitigating permanent deformation (rutting). These  
24 reinforcing materials can extend the service life of flexible pavements.

25 **Keywords:** 3-D model; ABAQUS; enhancement; flexible pavements; mechanical properties;  
26 permanent deformation; simulation.

## 27 **1. Introduction**

28 Due to increases in traffic volume, specifically heavy trucks, in terms of numbers of vehicles  
29 and high tyre pressures, above average demands are being placed on existing road pavements.  
30 Both horizontal and vertical stresses induced between pavement layers, result in permanent  
31 deformation (rutting) and crack formation [1]. Rutting is one of the main distresses that  
32 frequently occurs in flexible pavement overlays [2] which can be constructed using hot mix  
33 asphalt (HMA), warm mix asphalt (WMA) or cold mix asphalt (CMA). Cold mix asphalt is  
34 defined as bituminous materials which are prepared at ambient temperature by emulsifying the  
35 asphalt in water before blending with the aggregates. CMA has a number of benefits over  
36 HMA, but the main difference lies in the fact that CMA does not require any heating as it can  
37 be manufactured, laid and compacted without heating. In addition, CMA can offer the  
38 following advantages:

- 39 • CMA is not dependent upon warm weather.
- 40 • It can be mixed on site or off site.
- 41 • Eco-friendly option during all production processes made from water-based materials at  
42 ambient temperatures, which reduces emissions, energy consumption and toxic fumes.
- 43 • Cost-effective solution for paving or repairing rural roads that are nowhere near a hot mix  
44 plant, as minimal material and transportation costs required where CMA used in remote  
45 areas.

46 Although CMA provides both economic and environmental benefits in terms of removing the  
47 need for heating large amounts of aggregate [3, 4], it is rarely used due to its weak early  
48 strength, long curing time, high air voids and poor mechanical properties [4].

49 Reinforcing HMA and CMA with fibres can improve strength, bonding and durability [5-7].

50 Currently, natural and synthetic fibres are used as a reinforcing material in asphalt mixtures

51 because of their high stiffness and strength properties, and are considered the most appropriate  
52 reinforcing materials [1]. A variety of experimental research has been conducted to evaluate  
53 the effect of natural and synthetic fibres on the mechanical behaviour of bituminous mixtures  
54 in terms of hot mix asphalt. The results of these studies indicate that these fibres have a positive  
55 impact on the performance of bituminous mixtures [8-11], the performance of reinforced  
56 mixtures mainly affected by fibre length, content, type, diameter and surface texture [9, 12]. In  
57 consequence, in this research, several parameters pertaining to fibres; type, length and content,  
58 were considered and optimized when said fibres were added to CMA mixtures. Two different  
59 natural fibre types, jute and coir with 14 mm optimum fibre length and 0.35% fibre content,  
60 were used to improve the performance of the CMA mixtures [13].

61 In countries where high temperatures are the norm, pavement rutting is the major distress  
62 encountered in flexible pavements and considered to be one of the more complex issues in  
63 pavement structure [14]. It occurs due to the accumulation of permanent deformation on the  
64 pavement surface underneath the path of repeated wheel loadings. Such accumulated  
65 permanent deformation has been attributed to different variables including temperature, traffic  
66 volume, wheel load and repetition, tyre pressure, material properties and bituminous layer  
67 thickness [15]. Flexible pavement design methods are based on linear elastic calculations,  
68 however, new pavement design techniques are required to account for undesirable  
69 environmental conditions and heavy loading, these being common sources of rutting [16].  
70 However, given that flexible pavements are subjected to different loading and environmental  
71 conditions which impact on their performance, it is somewhat surprising that the impact of  
72 these aspects has not been fully simulated to date [16]. With specific reference to repeated  
73 loading, there is no technique currently available to investigate rutting on CMA pavements and  
74 no model available to predict permanent deformation for such pavements.

75 This research aims to predict the rutting behaviour of CMA mixtures reinforced with natural  
76 fibres. The Finite Element Method (FEM) is used to carry out the numerical analysis for this  
77 model. In finite element modelling, bituminous laboratory samples are tested to obtain the  
78 material properties that are required for the development of the viscoelastic model [17]. The  
79 rutting analysis is performed utilizing ABAQUS software.

80 Different techniques are available to predict rutting in bituminous mixtures such as finite  
81 difference methods [18], analytical methods [19], multilayer elastic theory [20], hybrid  
82 methods [21] and finite element methods [22, 23]. FEM has been used for bituminous materials  
83 but it does depend on experimental data as input. Allou, et al. [24] developed a 3-D linear  
84 viscoelastic model to characterize the dynamic modulus and Poisson's ratio of bituminous  
85 mixtures. Pérez, et al. [25] developed a 3-D finite element model to evaluate the response of  
86 rural road pavements when recycled in situ, using bitumen with two different added materials:  
87 75% natural aggregate and 25% reclaimed asphalt pavement, with and without 1% cement. Gu,  
88 et al. [26] evaluated the mitigation effect of geogrid-reinforced flexible pavements on rutting  
89 damage using a finite element model. The results showed that reinforced pavements have much  
90 better rutting resistance than unreinforced pavements.

91 The primary objectives of this study are to develop a 3-D finite element model to simulate the  
92 laboratory testing of CMA mixtures' wheel tracking tests for rutting and to relate the test results  
93 to the properties of the mixtures. This viscoelastic model was employed to assess loading time,  
94 strain, temperature and the properties of the mixture materials, to evaluate the behaviour of the  
95 CMA pavements.

## 96 **2. Viscoelasticity of cold mix asphalt**

97 Viscoelasticity is the property of a material that performs both viscous and elastic behaviours  
98 when subjected to deformation [27]. Viscous materials can resist shear stresses and show linear

99 strain patterns over time when loading is applied. Elastic materials strain instantaneously on  
100 loading, returning back to their original state without permanent deformation when the load is  
101 released. Asphalt mixtures have elements of both these characteristics and present time-rate  
102 dependent behaviour. They are considered viscoelastic materials when the deformation is  
103 small [28]. Bitumen is typically a viscous material when mixed with elastic aggregate to  
104 produce asphalt mixtures, hence viscoelasticity is expected. Viscosity can be represented by a  
105 dashpot, following the equation:

$$106 \quad \sigma(t) = \eta \frac{d\varepsilon(t)}{dt} \quad (1)$$

107 where  $\sigma(t)$  and  $\varepsilon(t)$  are stress and strain, respectively, and  $\eta$  is the viscosity. Elasticity can  
108 be represented by a spring, which follows the equations:

$$109 \quad \sigma(t) = E\varepsilon(t) \quad (2)$$

$$110 \quad \varepsilon(t) = D\sigma(t) \quad (3)$$

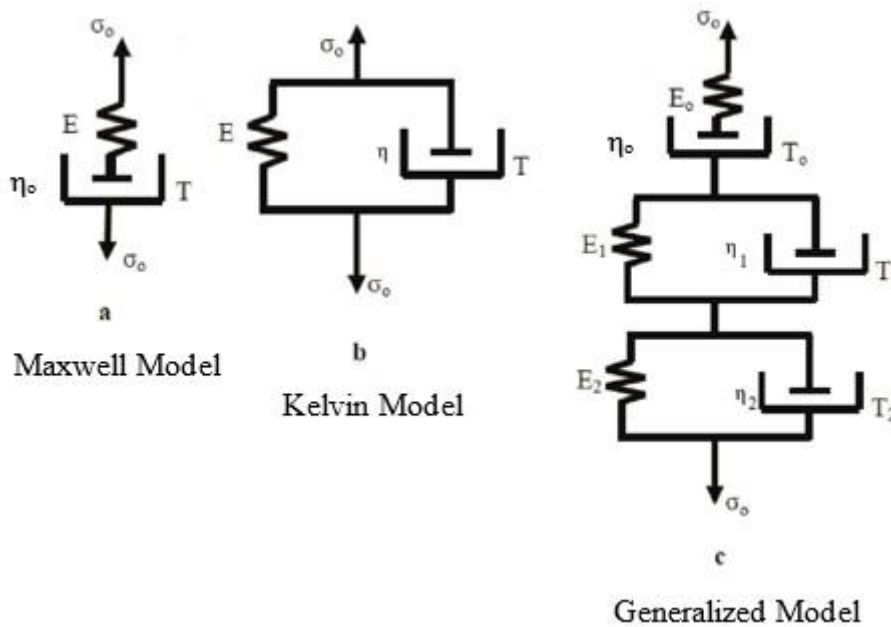
111 where  $E$  and  $D$  are the modulus and compliance of elasticity, respectively.

112 Different combinations of dashpots and springs represent a variety of viscoelastic models. For  
113 instance, the Maxwell model consists of one dashpot and one spring in series (Figure 1a), while  
114 the Kelvin-Voigt model consists of one dashpot and one spring in parallel (Figure 1b). After  
115 application of a single load, instantaneous and retarded elastic strains predominate and the  
116 viscous strain is negligible. However, under multiple load applications, the accumulation of  
117 viscous strain is the cause of permanent deformation [27]. Huang [27] suggested that a single  
118 Kelvin model is not adequate enough to cover the long period of time over which retarded  
119 strain takes place, and that a number of Kelvin models may be needed. In consequence, to  
120 describe the isotropic viscoelastic behaviour of bituminous mixtures, a generalized model has  
121 been used in this study. This model consists of one Maxwell model and two Kelvin models

122 connected in a series as shown in Figure 1c. The total strain at time  $t$  of the generalized model  
 123 is given as follows [29]:

$$124 \quad D(t) = \frac{\sigma}{E_0} \left( 1 + \frac{t}{T_0} \right) + \sum_{i=1}^N \frac{\sigma}{E_i} \left( 1 - e^{-\frac{t}{T_i}} \right) \quad (4)$$

125 where  $D(t)$  is the creep compliance;  $E_0$  the initial elastic modulus at time zero;  $T_0$  the relaxation  
 126 time;  $t$  the loading time;  $T_i$  the retardation time ( $T_i = \eta / E$ );  $E_i$  the elastic modulus at any time  
 127 and  $N$  the number of Kelvin models in the Prony series model. This equation is also known as  
 128 a Prony series expansion.



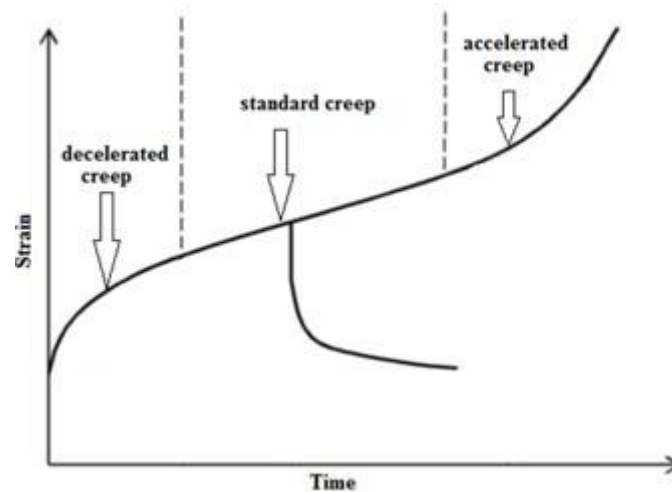
129  
 130 Figure 1. Mechanical models for viscoelastic materials

131 The phenomenon of permanent deformation (rutting) can be evaluated by carrying out creep  
 132 and relaxation tests [30]. Both creep compliance  $D(t)$  and relaxation modulus  $E(t)$  are required  
 133 to develop a viscoelastic model; creep compliance is required to predict deformation and the  
 134 relaxation modulus to determine pseudo strain. In this study, Prony series coefficients have  
 135 been fitted to experimental data to represent the viscoelastic (time-dependent) properties of the

136 bituminous mixtures. The experimental data were obtained from creep and relaxation tests for  
137 reinforced and unreinforced cold mix asphalt mixtures.

138 The creep and relaxation test for asphalt mixtures, a typical strain-time curve, can be divided  
139 into three distinct strain stages: decelerated creep, the first stage where the strain rate decreases;  
140 standard creep, the second stage with a constant strain rate and accelerated creep, the third stage  
141 which sees an increase in strain rate. These three stages of asphalt mixture behaviour are shown  
142 in Figure 2. The total strain in asphalt mixtures usually consists of four constituents: (1)  
143 recoverable elastic strain which is time-independent; (2) recoverable viscoelastic strain which  
144 is time-dependent; (3) irrecoverable plastic strain which is time-independent, and (4)  
145 irrecoverable viscoplastic strain which is time-dependent. During recovery time, elastic strain  
146 is instantaneously recovered deformation while delayed recovered deformation is viscoelastic  
147 strain. Viscoelastic strain needs adequate time to fully recover. Permanent strain is the  
148 combination of both plastic and viscoplastic strains.

149 The objective of this study is to investigate a viscoelastic model that can entirely characterize  
150 the first two stages of creep deformation behaviour, for both reinforced and conventional cold  
151 mix asphalt mixtures, through a series of creep and relaxation tests.



152  
153

Figure 2. Creep and relaxation behaviour at constant stress



154 **3. Experimental methods**

155 3.1 Materials

156 The conventional (CON) cold mix asphalt (CMA) mixture was made of aggregates of gradation  
157 14 mm, a close-graded surface course, in according with the European Committee for  
158 Standardization-part 1 [31], as presented in Table 1. Based on the British Standard [31], the  
159 selected aggregate is one of the most common aggregate used in the production of asphalt and  
160 it is considered hard, durable, clean, have suitable shape, provide a level of skid resistance and  
161 resist permanent deformation. In addition, this selection was in order to ensure an appropriate  
162 interlock between the particles in the mixtures. Cationic, slow-setting (B3), bituminous  
163 emulsion with 50% bitumen content (C50B3), was used as the binding agent for the aggregates.  
164 The supplier of this emulsion (Jobling Purser, Newcastle, UK) has used another commercial  
165 name as a cold asphalt binder (CAB 50) and it is based on a 40/60 penetration grade base  
166 bitumen. Table 2 shows the properties of the selected bitumen emulsion. Two types of natural  
167 fibres were used as reinforcement materials; jute (JUT) and coir (COI) fibres. According to the  
168 laboratory results, the reinforced mixtures were made with the optimum fibre content and  
169 length, 0.35% and 14 mm, respectively.

170 Table 1. Selected mix gradation

Sieve size (mm)	14	10	6.3	2	1	0.063
Passing (%)	100	80	55	28	20	6

171

172

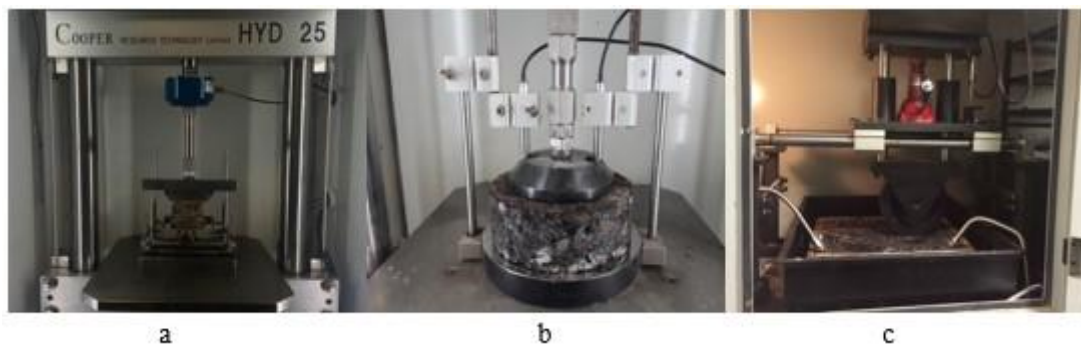
Table 2. Properties of (CAB 50) bitumen emulsion

Property	Value	Standard
Type	Cationic	
Appearance	Black to dark brown liquid	
Breaking behaviour	110-195	EN 13075-1
Base bitumen Penetration (0.1 mm)	50	EN 1426
Softening Point (°C)	50	EN 1427
Bitumen content, (%)	50	EN 1428
Viscosity (2mm at 40°C)	15-70	EN 12846
PH	5	
Boiling point, (°C)	100	
Adhesiveness	≥ 90%	EN13614
Relative density at 15 °C, (g/ml)	1.05	
Particle surface electric charge	positive	EN 1430
Density (g/cm <sup>3</sup> )	1.016	

173

174 3.2 Indirect tensile stiffness modulus test

175 The indirect tensile stiffness modulus test (ITSM), is a non-destructive test mainly used to  
176 evaluate the stiffness modulus of asphalt mixtures (see Figure 3a). ITSM at 20°C has been used  
177 to optimize the length of the fibres and the fibre and emulsion content. Four different testing  
178 temperatures, 5°C, 20°C, 45°C and 60°C, were used to assess the susceptibility to temperature  
179 of the mixtures. This test is carried out in accordance with the European Committee for  
180 Standardization, part 26 [32].



181

182 Figure 3. Laboratory equipment

183 3.3 Creep and relaxation test

184 The creep test at 5°C, 20°C, 45°C and 60°C, was used to study the influence of reinforced and  
185 unreinforced mixtures on creep performance to assess their viscoelastic properties (Figure 3b).

186 The test was conducted under 0.1 MPa stress in accordance with the European Committee for  
187 Standardization, part 25 [33].

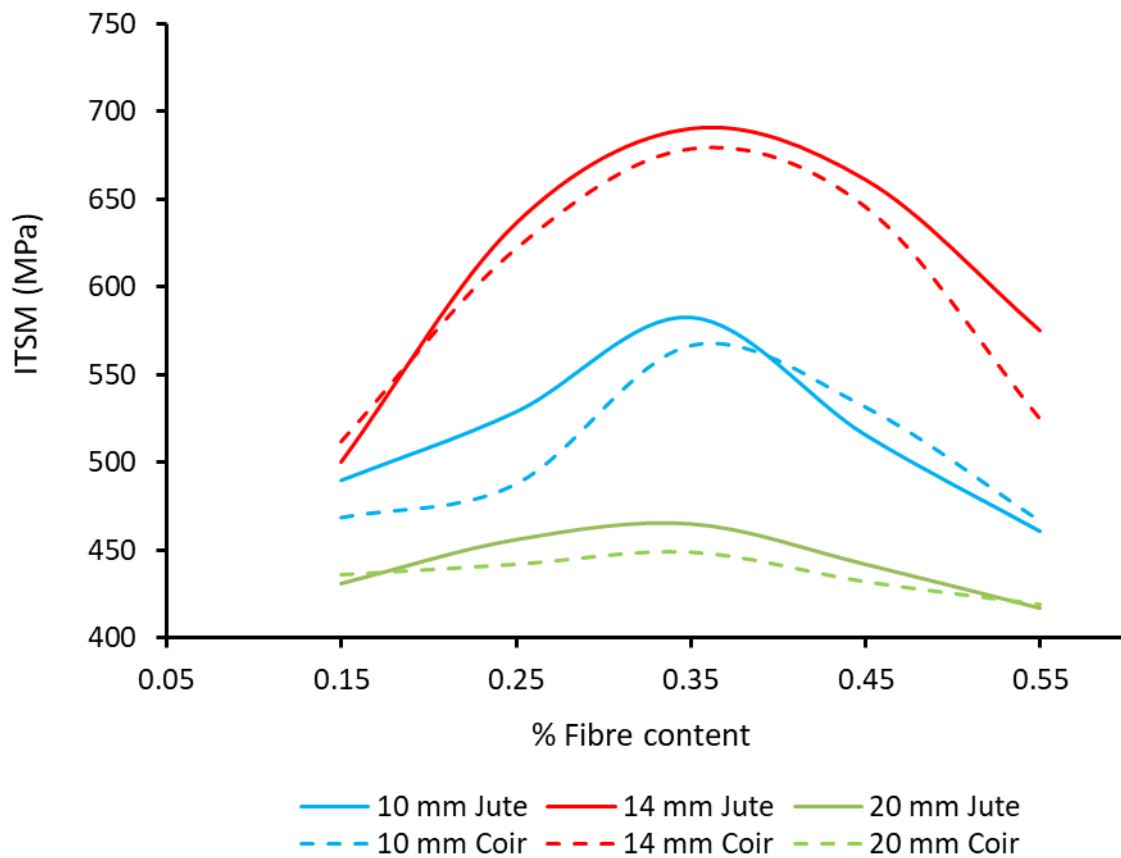
### 188 3.4 Wheel track test

189 The laboratory wheel track test was used for the asphalt mixtures to assess resistance to rutting  
190 of hot and cold mix asphalt mixtures [34, 35], following the European Committee for  
191 Standardization, part 22 [36]. This test is used to validate the model results in terms of rut depth  
192 and deformation shape (Figure 3c). Prior to carrying out the tests, the loose bituminous  
193 mixtures were mixed and compacted in a steel mould under a steel roller compactor, resulting  
194 in a solid slab measuring 400 mm (length)  $\times$  305 mm (width)  $\times$  50 mm (thickness). The  
195 specimens then were kept in the mould for 24 hours at room temperature (20°C). Following  
196 this, the slabs were cured for 14 days, inside a ventilated oven at 40°C, to achieve full curing  
197 [34]. This curing temperature is significant as it needs to be less than the bitumen softening  
198 point (50°C) and thus prevent the bitumen from ageing [34]. Slab specimens were tested to  
199 measure rut depth in both the reinforced and conventional cold mix asphalts (close-graded  
200 surface course). Wheel track testing was conducted at 45°C and 60°C, under application of 700  
201 kPa stress. Three slabs of each mixture type were tracked using the wheel tester.

## 202 **4. Fibres optimisation**

203 The Indirect Tensile Stiffness modulus is regarded as key when evaluating the effect of  
204 different fibre lengths and contents on CMA mixture performance, taking into account the  
205 effect of curing time and condition. Figure 4 shows that ITSM initially increases then  
206 decreases, with increasing fibre content, for all fibre lengths and types. The CMA mixture  
207 reinforced with 0.35% fibre content by weight of dry aggregate, had a higher ITSM than the  
208 other mixtures for all fibre lengths. This is in agreement with other researchers Chen, et al. [9]  
209 and Xu, et al. [37] who recommend that the optimum fibre content should be between 0.3%  
210 and 0.4%, based on the results from similar tests. 14 mm long fibres, cured for 2 days,

211 developed the ITSM of the reinforced CMA mixtures to the maximum value. This indicates  
 212 that the reinforced mixture with 14 mm fibre length and 0.35% content adheres well to the  
 213 bitumen [1]. According to Liu, et al. [38], short fibres (10 mm) cannot properly reinforce  
 214 mixtures that have a larger size of aggregate (maximum 14 mm) while long fibres (longer than  
 215 the maximum size of the aggregate) can lead to loss in mixture strength because these fibres  
 216 tend to lump together during the mixing process. The results found here were similar to those  
 217 found in the literature [39]. Because of the use of an appropriate length of fibre (14 mm in this  
 218 research), the placement and distribution of this fibre in the bituminous mixture, produced  
 219 enhanced interlocking between the fibre and the paste, hence the lateral strain was delayed and  
 220 the mixture strength improved [40].



221  
 222 Figure 4. Fibre optimisation at 20 °C after 2 days

223 **5. Finite element model development**

224 Different techniques are available to predict flexible pavement deformation such as multilayer  
225 elastic theory, boundary element methods, analytical methods, hybrid methods, finite  
226 difference methods and finite element methods (FEM) [14]. FEM has been used successfully  
227 for flexible pavement performance analysis and has been found suitable for application to the  
228 complex behaviour of composite pavement materials. Furthermore, using three-dimensional  
229 (3D) finite element models can solve the problems that cannot be solved by two-dimensional  
230 (2D) models under repeated loading. Therefore, in this study, a 3D finite element model has  
231 been adopted for analysis to simulate the natural fibre reinforced CMA mixtures. This model  
232 includes consideration of viscoelastic pavement properties and moving load applications to  
233 accurately characterize the time, rate and temperature dependent responses of the bituminous  
234 layer.

235 The commercial finite element software ABAQUS was used to build this model to evaluate the  
236 changes in pavement response properties. This program has been widely used in other research  
237 to model hot mix asphalt pavements systems because this type of model can include  
238 consideration of the behaviour of viscoelastic materials under repeated loadings: to date this  
239 same model has not been applied to CMAs.

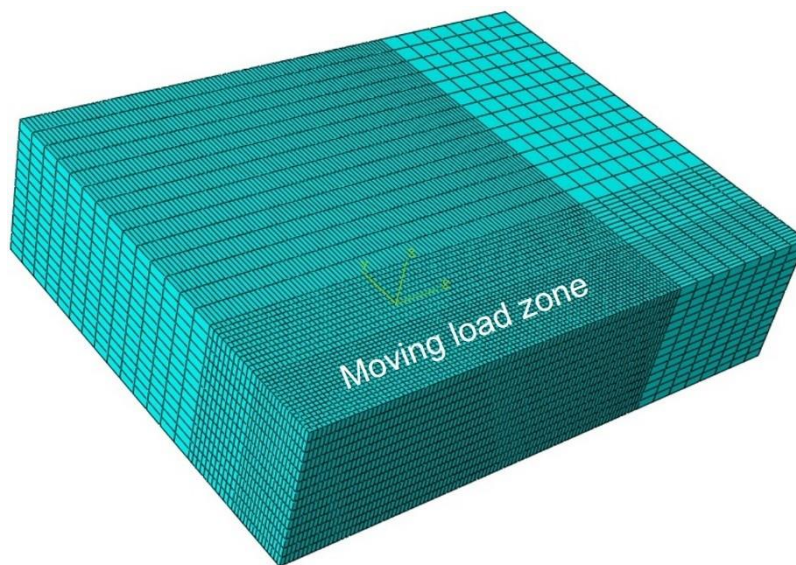
#### 240 5.1 Model geometry, boundary conditions and meshing.

241 Depending on the nature of the finite element analysis, it is essential to find suitable dimension,  
242 mesh and boundary conditions for the model to be analysed. Therefore, to optimize  
243 computation times and provide results comparable to the experimental data, the number of  
244 trials, mesh size and density, number of elements and suitable dimensions were determined.

245 The geometry of the FEM is based on a section (a slab) of a wheel tracking test. The surface  
246 of the pavement is assumed to be symmetrical (x and y-axes), therefore, a quarter of the model  
247 is used to reduce the cost of the analysis [24, 25, 41]. The model geometry consists of a  
248 bituminous layer with a depth of 5 cm, length and width of 20 and 15.25 cm, respectively,

249 positioned over a fixed steel plate. The model boundary conditions were selected to exert a  
250 significant influence on the predicted response of the pavement. These boundaries are applied  
251 to the all the edges, or faces, of the structural pavement geometric model to control  
252 displacement in a horizontal direction on the vertical edge, perpendicular to the layer surface.  
253 Thus, the bottom of the layer moves in all directions, while the horizontal and vertical  
254 deflections can be predicted in all other planes.

255 An 8-node brick element was used for the generation of the mesh. In order to determine a  
256 suitable size of element to ensure the desired degree of accuracy for the developed model,  
257 different mesh densities were applied. It can be seen from Figure 5 that the densest mesh was  
258 used in the areas under, and near to, the load applications, whilst relatively coarser meshes  
259 were employed further away from the loading area, in both directions. A mesh sensitivity  
260 analysis was conducted to determine the optimum element size for the fine mesh. According  
261 to this analysis, the smallest element length is 1.5 mm. The finite element mesh contains 58548  
262 C3D8R (Continuum 3-Dimensional 8 node elements with reduced integration) brick elements  
263 and 64890 nodes.



264

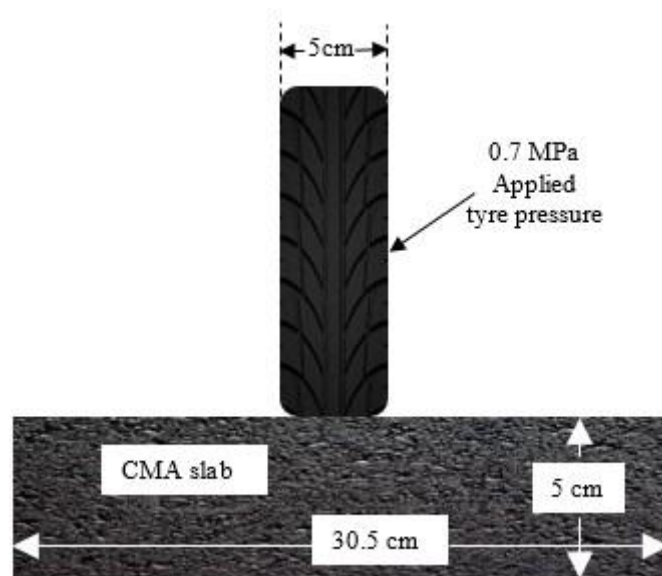
265

Figure 5. 3-D finite element mesh for pavement simulation

266

## 5.2 Loading configuration

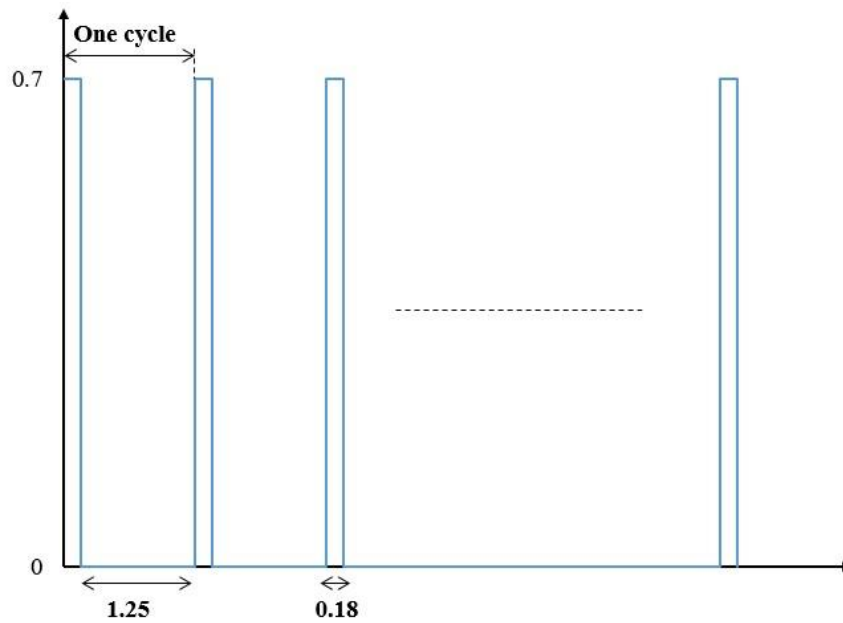
267 The wheel tracking test results were used to validate the model while wheel loading was used  
268 to investigate pavement response. The viscoelastic effect of the bituminous layer is an essential  
269 facet regarding the analysis of flexible pavements in terms of CMA. For that reason, in the  
270 FEM, it is important to consider time and loading rate dependency in addition to temperature.  
271 In order to properly characterize these factors, cyclic and static loadings were applied to the  
272 surface of the finite elements, seen as a small rectangle which represents a tyre footprint. [42].  
273 This load transfers to the pavement surface through contact pressure between the tyre and  
274 pavement surface. The contact pressure is equal to the tyre pressure on the road surface [43].  
275 A total of 700 kPa pressure loads were applied and distributed uniformly over the contact area,  
276 to simulate the load of a wheel tracking test with a speed of 0.6 km/h, as shown in Figure 6.  
277 This pressure is applied repeatedly to the pavement surface over many cycles. During each  
278 cycle (1.44 s), the load is applied for 0.18 s to simulate a vehicle speed of about 0.6 km/h. The  
279 load is then removed for 1.26 s as schematically shown in Figure 7. A relatively high  
280 temperature (60°C) was used to examine the effect of high temperature on the flexible  
281 pavements.



282

283

Figure 6. Dimensional cross-section of slab modelling



284

285

Figure 7. Schematic of the applied repeated loading

286 5.3 Material characterization

287 The ABAQUS software used in this research has the capacity to analyse complex time and rate  
 288 dependent, viscoelastic problems. For the viscoelastic analysis of bituminous materials, shear  
 289  $G(t)$  and/or bulk  $K(t)$  moduli are required in most finite element modelling as viscoelastic  
 290 material property inputs. These properties can be calculated (using equation 4) from the creep  
 291 test at certain temperature using the Prony series. This is a mechanical representation of the  
 292 viscoelastic material behaviour of flexible pavements [44]. Flexible pavement material is  
 293 homogeneous and isotropic and the Poisson's ratio does not change with time [45]. Poisson's  
 294 ratio has therefore been considered a constant (0.35). This the most suitable assumption for  
 295 bituminous mixtures as it provides reasonable and accurate time and rate dependent responses  
 296 of viscoelastic materials [46]. Elastic modulus of different CMA mixtures at different  
 297 temperatures were measured using ITSM test. The Prony series parameters and moduli of  
 298 elasticity were successfully calculated based on the experimental results, as given in Table 3,  
 299 after 14 days of curing time.



300 Table 3. Elastic and viscoelastic properties of different CMA mixtures at different temperatures

		Viscoelastic material coefficients					
		Temperatures (°C)					
		60			45		
		$D_i$ (1/kPa)			$D_i$ (1/kPa)		
$i$	$\tau_i$ (s)	CON	JUT	COI	CON	JUT	COI
1	0.1	$6.91 \times 10^{-6}$	$4.86 \times 10^{-6}$	$4.65 \times 10^{-6}$	$1.14 \times 10^{-5}$	$2.75 \times 10^{-6}$	$2.69 \times 10^{-5}$
2	1	$6.12 \times 10^{-5}$	$3.36 \times 10^{-5}$	$4.41 \times 10^{-5}$	$1.90 \times 10^{-5}$	$2.14 \times 10^{-5}$	$4.05 \times 10^{-5}$
3	10	$1.54 \times 10^{-4}$	$8.52 \times 10^{-5}$	$1.04 \times 10^{-4}$	$4.08 \times 10^{-5}$	$6.71 \times 10^{-5}$	$8.03 \times 10^{-5}$
4	100	$2.09 \times 10^{-4}$	$1.39 \times 10^{-4}$	$1.27 \times 10^{-4}$	$7.43 \times 10^{-5}$	$8.67 \times 10^{-5}$	$1.31 \times 10^{-4}$
5	1000	$2.62 \times 10^{-4}$	$1.74 \times 10^{-4}$	$1.42 \times 10^{-4}$	$1.08 \times 10^{-4}$	$1.15 \times 10^{-4}$	$1.72 \times 10^{-4}$
Modulus of elasticity $E$ (MPa)		35	311	255	100	417	324

		Viscoelastic material coefficients					
		Temperatures (°C)					
		20			5		
		$D_i$ (1/kPa)			$D_i$ (1/kPa)		
$i$	$\tau_i$ (s)	CON	JUT	COI	CON	JUT	COI
1	0.1	$3.66 \times 10^{-6}$	$1.10 \times 10^{-6}$	$6.30 \times 10^{-6}$	$8.81 \times 10^{-6}$	$7.68 \times 10^{-6}$	$9.11 \times 10^{-6}$
2	1	$5.18 \times 10^{-6}$	$1.52 \times 10^{-6}$	$1.69 \times 10^{-5}$	$7.24 \times 10^{-5}$	$4.34 \times 10^{-5}$	$5.53 \times 10^{-5}$
3	10	$3.90 \times 10^{-5}$	$3.05 \times 10^{-5}$	$3.69 \times 10^{-5}$	$9.63 \times 10^{-5}$	$6.02 \times 10^{-5}$	$8.78 \times 10^{-5}$
4	100	$5.67 \times 10^{-5}$	$5.08 \times 10^{-5}$	$5.16 \times 10^{-5}$	$5.16 \times 10^{-4}$	$9.79 \times 10^{-5}$	$4.33 \times 10^{-4}$
5	1000	$7.40 \times 10^{-5}$	$5.21 \times 10^{-5}$	$6.28 \times 10^{-5}$	$8.25 \times 10^{-4}$	$2.95 \times 10^{-4}$	$8.19 \times 10^{-4}$
Modulus of elasticity $E$ (MPa)		464	1021	890	581	1876	1634

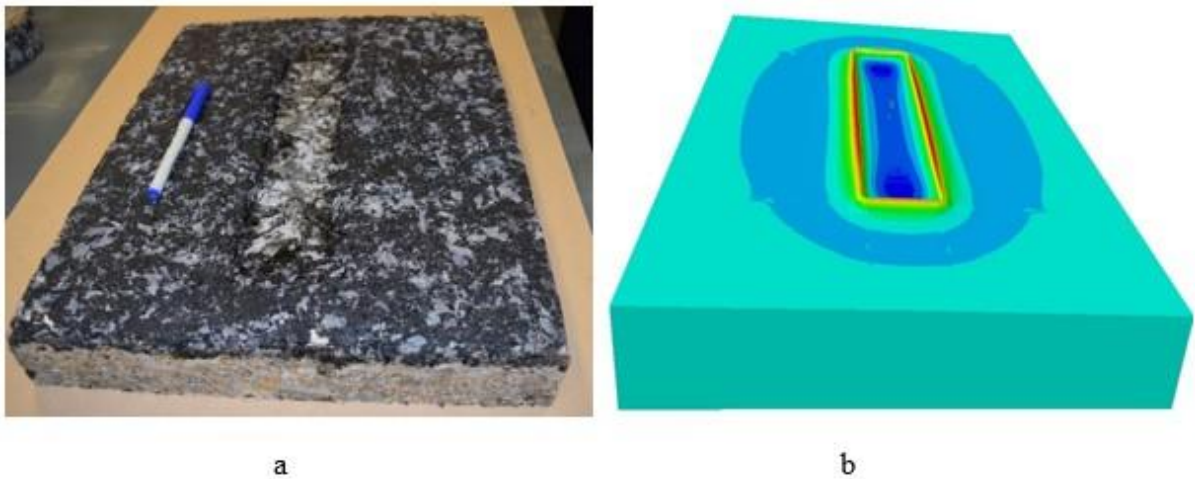
301

302 **6. Results and Discussion**

303 6.1 Model validation

304 The responses of the CMA, predicted by the viscoelastic model developed for two different  
305 natural fibres, were validated against those from the wheel tracking tests. The wheel tracking  
306 tests were conducted for CMA mixtures, with and without fibres, to calculate rutting at the  
307 surface of the bituminous layer. Transverse surface permanent deformation was calculated after  
308 3472 load applications. A similar set of experiments were conducted using the finite element  
309 model to compare the actual measurements of rutting (permanent deformation) with the rutting  
310 values obtained from the model. The magnitude of permanent deformation at the surface of the  
311 CMA layer, is the most significant factor characterizing the rutting performance of flexible

312 pavements. Rutting transfer functions are the functions of shear and tensile strain at the surface  
313 of the bituminous layer, under applied wheel loads. It is therefore imperative to accurately  
314 predict deformation response characteristics at the surface of the CMA layer for more  
315 appropriate evaluation of pavement rutting. The CMA mixtures were conducted at 45°C and  
316 60°C during the wheel tracking tests. Based on the comparison of time-deformation, peak  
317 deformation and transverse surface deformation, it can be seen that the FEM-simulated-CMA  
318 response is close to the lab response, as shown in Figure 8. Therefore, it can be claimed that  
319 the model is validated and ready for further parametric study.

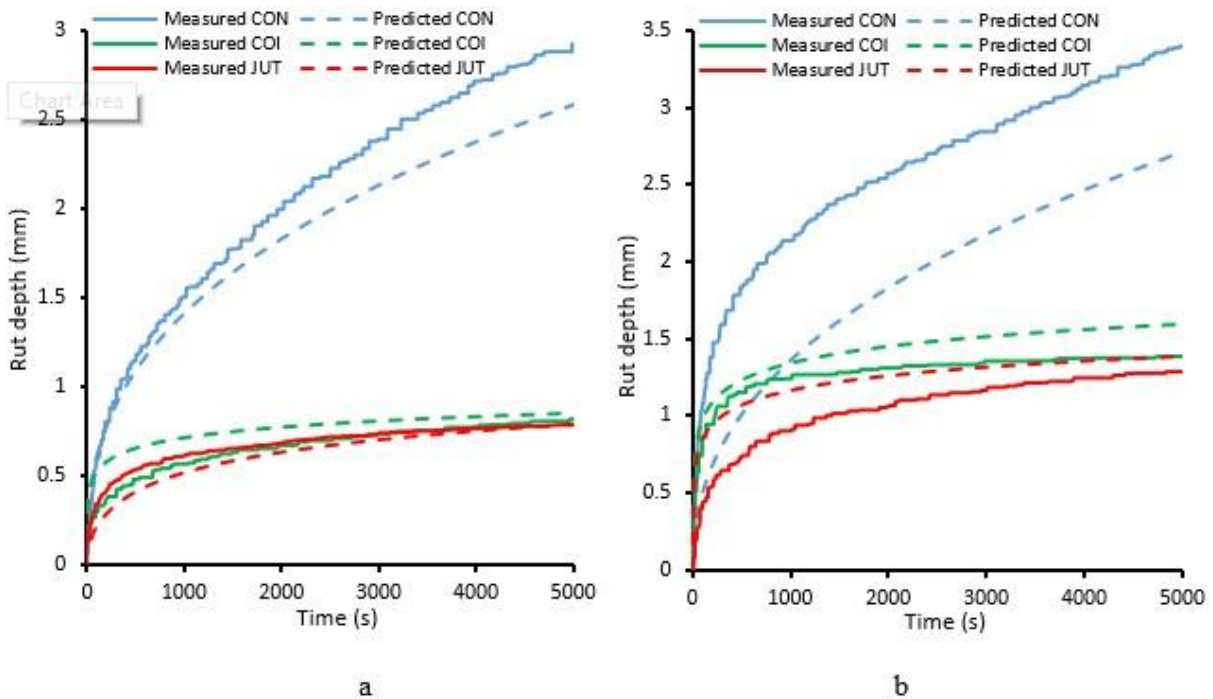


320  
321 Figure 8. Deformed shape of conventional CMA at 45°C (a) measured, and (b) predicted

### 322 6.2 Rutting in cold mix asphalt mixtures

323 Figure 9 shows the rutting measured on the surface of the CMA layer, under the centre of the  
324 moving wheel path, and those predicted by the viscoelastic model for both reinforced (by jute  
325 and coir fibres) and conventional (no treatment) mixtures, at two different temperatures (45°C  
326 and 60°C). The predicted rutting matches well with the measured ruts, even though some  
327 variations were observed (between the predicted and measured rutting) between mixture types  
328 and temperature. This small vibration between the predicted and measured rutting is because  
329 of the model assumes that the material properties are uniform and homogenous, whilst in reality  
330 the mixtures include some voids and different aggregate interlocks. Also, in reality, the

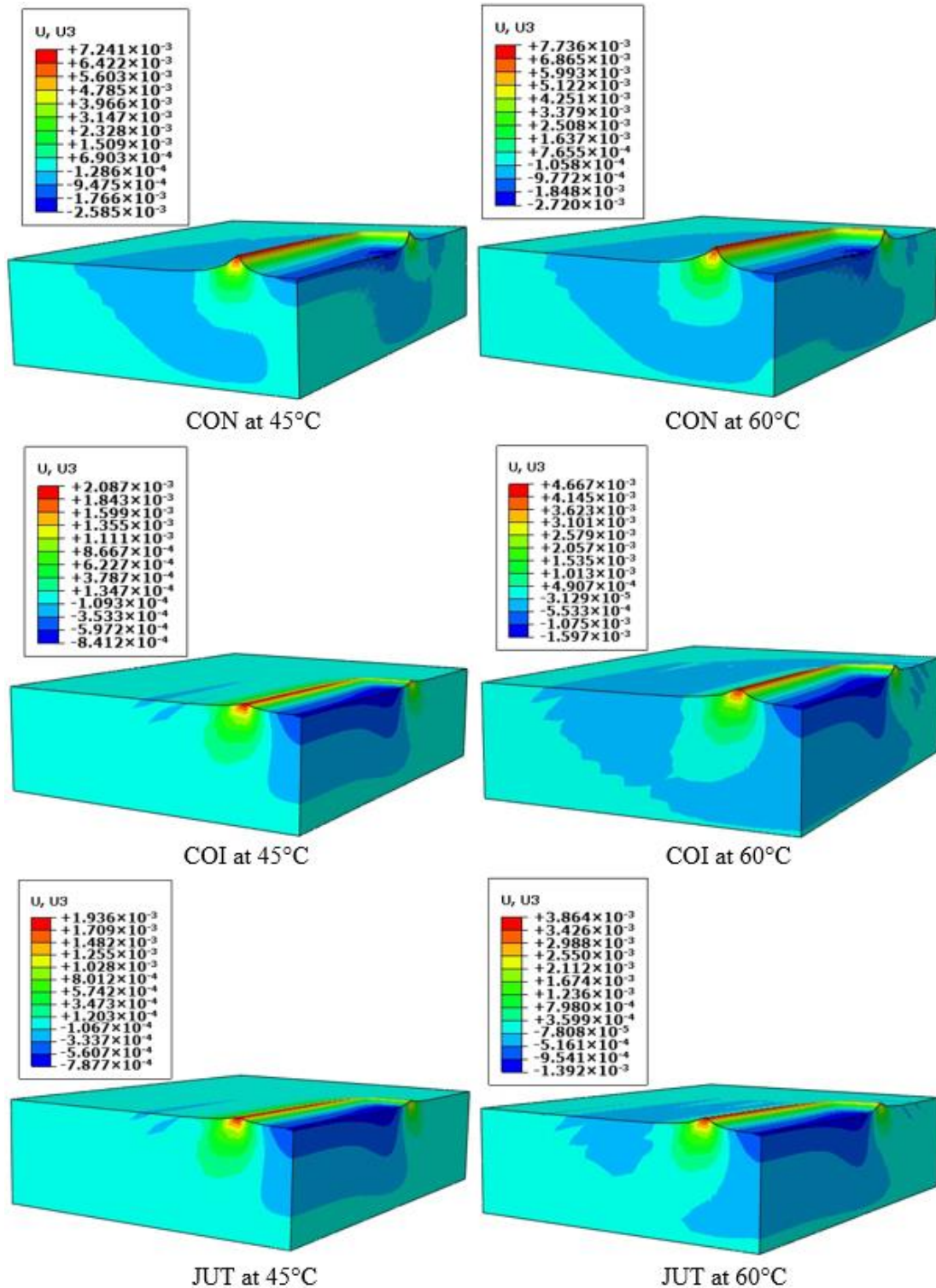
331 temperature and viscosity of the mixtures can not be distributed equally for the whole mixture  
 332 and this can not be modelled because of the difficulty of setting different temperatures and  
 333 viscosities for each particles of the mixture. However, these discrepancies do not affect the  
 334 validation of the FE model. It is interesting to note the distinctive difference in the rutting due  
 335 to the different fibres used. The measured and predicted permanent deformation of the  
 336 bituminous layer that occurs along the moving area under the wheel path, is calculated as the  
 337 average deformation along, and under, the wheel path. The results clearly show that the CMA  
 338 with jute and coir fibres induces reduced rutting on the bituminous surface layer, this positively  
 339 affecting the rutting resistance of flexible pavements.



340 a b  
 341 Figure 9. Predicted vs. measured rutting at the top of the pavements (a) at 45°C and (b) 60°C

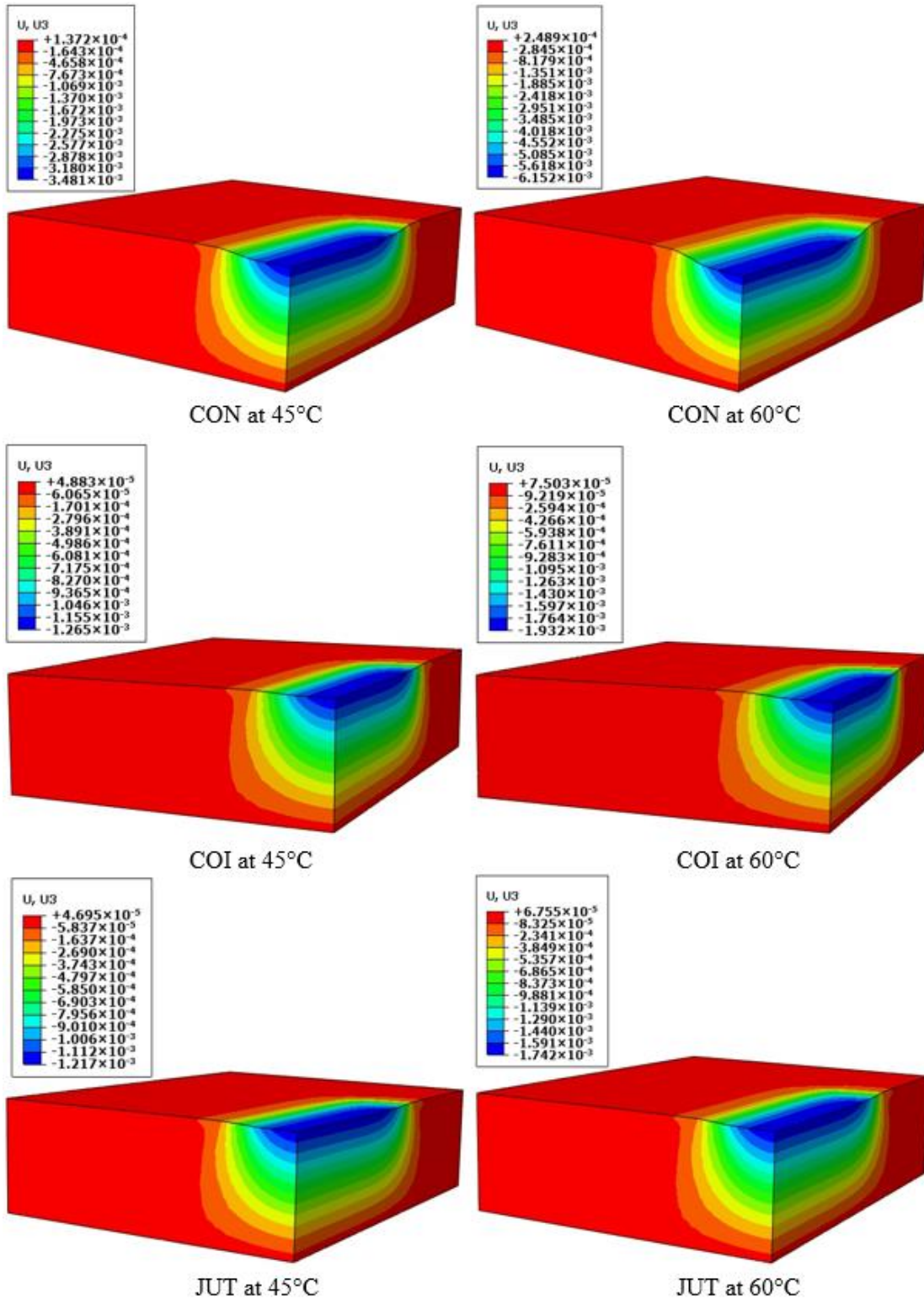
342 The permanent deformation of the different CMA mixes, after 3472 cycles (about 5000 s), are  
 343 illustrated in Figure 10. The results of the equivalent static loading condition (5000 s loading)  
 344 on the same model, are also presented in Figure 11. Both different loading conditions were  
 345 performed following the same order of permanent deformation resistance; the CMA mixtures  
 346 reinforced with jute, have the smallest rut depth followed by the coir fibre mix. The

347 conventional CMA mixtures have the maximum rut depth. The permanent deformation found  
 348 in the static loading condition is greater than that of the cyclic loading condition for all mixture  
 349 types because there is no rest interval to let mixtures recover (viscoelastic properties) in the  
 350 static loading condition.



351  
 352

Figure 10. Permanent deformation for cyclic loading at 45°C and 60°C



353

354

Figure 11. Permanent deformation for static loading at 45°C and 60°C

355

Because the elastic modulus of conventional CMA is less than the modulus of the reinforced

356

CMA mixtures, its rut depth is greater. The elastic modulus and viscoelastic properties of

357

different CMA mixtures (as shown in Table 3) have a significant effect on rut depth.

### 358 6.3 Sensitivity analysis

359 After the rutting analysis and validation of the model, a sensitivity analysis was performed to  
360 investigate the effect of different factors on flexible pavements response, dependent on mixture  
361 type.

#### 362 6.3.1 Temperature attributes

363 The permanent deformation of flexible pavements is closely related to pavement temperature  
364 as variation in temperature effects stiffness modulus and shear stress. Rutting resistance  
365 increases when the pavement temperature is low (around 0°C) because of the high stiffness of  
366 asphalt pavements [47]. The variation in pavement rutting for different temperatures (20°C and  
367 5°C) is shown in Figure 12. As expected from the model, the CMA mixtures at low  
368 temperatures, show lower permanent deformation than at high temperatures. Given there is a  
369 significant effect of temperature on rutting, design procedures and analysis should include  
370 actual pavement temperatures.

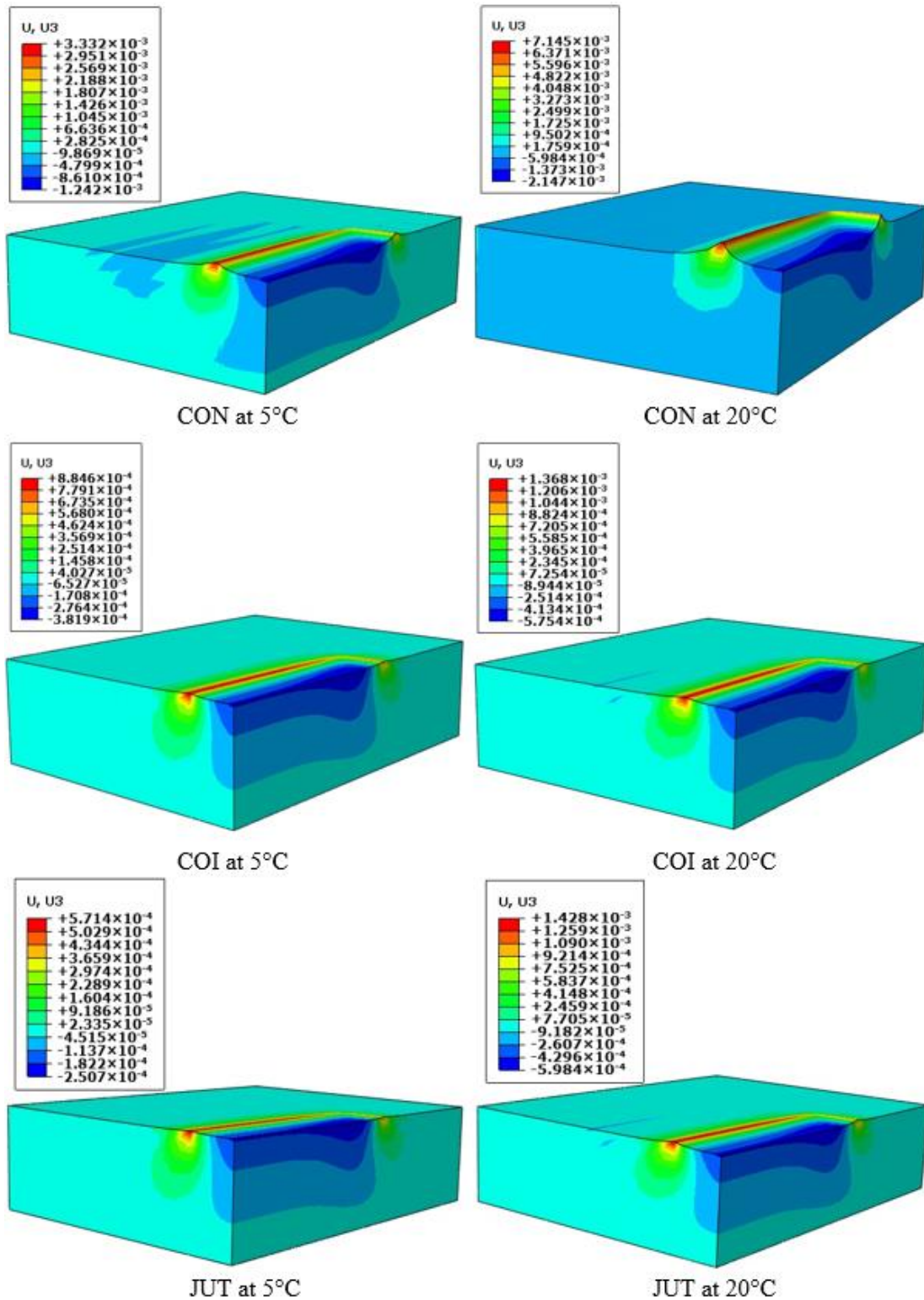


Figure 12. Permanent deformation for cyclic loading at 5°C and 20°C

371

372

373 6.3.2 Load and vehicle speed attributes

374 Zhi, et al. [48] stated that static loads are more damaging to asphalt pavements than moving

375 loads. A comparison was carried out, using this model, on the effect of different traffic speeds

376 (5, 30 and 60 Km/h) on reinforced and unreinforced CMA. Cumulative pavement rutting on  
 377 the top of the asphalt layer at 30 km/h, is significantly less than that at 5 km/h. The rutting  
 378 variation between 30 km/h and 60 km/h is relatively small, as shown in Table 4. The loading  
 379 time for each cycle (1.44 s), is dependent on vehicle speed. It is 0.0216 s at 5 km/h, 0.0036 s at  
 380 30 km/h and 0.0018 s at 60 km/h.

381 Table 4. Maximum rut depth for different vehicle speeds after 5000 s.

Temperature (°C)	Vehicle speed (km/h)	Max. rut depth (mm)		
		CON	COI	JUT
60	5	2.75	1.31	1.25
	30	1.22	0.79	0.68
	60	0.98	0.60	0.55
45	5	2.20	0.72	0.63
	30	0.87	0.44	0.38
	60	0.66	0.38	0.32
20	5	1.63	0.48	0.41
	30	0.57	0.31	0.21
	60	0.51	0.28	0.18
5	5	0.74	0.26	0.20
	30	0.29	0.12	0.09
	60	0.26	0.10	0.07

382

### 383 7. Conclusion

384 This research presents a viscoelastic model for asphalt pavements, using a cold mix asphalt  
 385 subjected to static and multiple-axle loads. This model was developed using the Prony series  
 386 parameter properties of CMA mixtures to simulate a laboratory wheel-tracking test. In order to  
 387 compare numerical predictions to laboratory measured rut depth values, reinforced and  
 388 unreinforced CMA mixtures were also tested in the laboratory. A good level of agreement was  
 389 obtained between the predicted rutting and experimental results, measured on the surface of  
 390 the bituminous pavements. The validated model was used to evaluate the permanent  
 391 deformation of different CMA mixtures, subjected to different tyre speeds and temperatures.



392 Based on laboratory tests and FEM analyses, some important observations and conclusions can  
393 be made:

- 394 • The generalized model can be used effectively to analyse the rutting characteristics in  
395 CMA mixtures. The viscoelastic parameters of the generalized model fit with the  
396 procedure described in this research.
- 397 • According to the results, the developed model can accurately predict the rutting  
398 behaviour of reinforced and unreinforced CMA mixtures, under different stresses and  
399 temperatures.
- 400 • Tyre speed, temperature, loading and bituminous material properties have an effect on  
401 the depth of rutting of CMA mixtures.
- 402 • FEM analysis indicates that at high temperatures and static loading conditions,  
403 maximum rutting depth occurs.
- 404 • The results show that jute and coir fibres have positive effects on the mechanical  
405 behaviour of CMA mixtures.

#### 406 **Acknowledgments**

407 The first author would like to express his gratitude to the Ministry of Higher Education &  
408 Scientific Research, Iraq and Al Muthanna University, Iraq for financial support. The authors  
409 also wish to thank David Jobling-Purser, Steve Joyce, Neil Turner and Richard Lavery for  
410 providing the materials for this research project.

#### 411 **References**

- 412 [1] Abiola, O.S., et al., *Utilisation of natural fibre as modifier in bituminous mixes: A review*.  
413 *Construction and Building Materials*, 2014. **54**: p. 305-312.
- 414 [2] Mahrez, A. and Karim, M.R., *Fatigue characteristics of stone mastic asphalt mix reinforced with*  
415 *fiber glass*. *International Journal of Physical Sciences*, 2010. **5**(12): p. 1840-1847.

- 416 [3] Dulaimi, A., et al., *High performance cold asphalt concrete mixture for binder course using alkali-*  
417 *activated binary blended cementitious filler*. Construction and Building Materials, 2017. **141**: p.  
418 160-170.
- 419 [4] Dulaimi, A., et al., *New developments with cold asphalt concrete binder course mixtures*  
420 *containing binary blended cementitious filler (BBCF)*. Construction and Building Materials, 2016.  
421 **124**: p. 414-423.
- 422 [5] Wu, S.-p., et al., *Effect of fiber types on relevant properties of porous asphalt*. Transactions of  
423 Nonferrous Metals Society of China, 2006. **16**: p. s791-s795.
- 424 [6] Ye, Q., Wu, S., and Li, N., *Investigation of the dynamic and fatigue properties of fiber-modified*  
425 *asphalt mixtures*. International Journal of Fatigue, 2009. **31**(10): p. 1598-1602.
- 426 [7] Ferrotti, G., Pasquini, E., and Canestrari, F., *Experimental characterization of high-performance*  
427 *fiber-reinforced cold mix asphalt mixtures*. Construction and Building Materials, 2014. **57**: p. 117-  
428 125.
- 429 [8] Yang, J.-M., Kim, J.-K., and Yoo, D.-Y., *Effects of amorphous metallic fibers on the properties of*  
430 *asphalt concrete*. Construction and Building Materials, 2016. **128**: p. 176-184.
- 431 [9] Chen, H., et al., *Evaluation and design of fiber-reinforced asphalt mixtures*. Materials & Design,  
432 2009. **30**(7): p. 2595-2603.
- 433 [10] Saeid, H., Saeed, A., and Mahdi, N., *Effects of rice husk ash and fiber on mechanical properties*  
434 *of pervious concrete pavement*. Construction and Building Materials, 2014. **53**: p. 680-691.
- 435 [11] Guoming, L., Weimin, C., and Lianjun, C., *Investigating and optimizing the mix proportion of*  
436 *pumping wet-mix shotcrete with polypropylene fiber*. Construction and Building Materials, 2017.  
437 **150**: p. 14-23.

- 438 [12] Abtahi, S.M., Sheikhzadeh, M., and Hejazi, S.M., *Fiber-reinforced asphalt-concrete – A review.*  
439 Construction and Building Materials, 2010. **24**(6): p. 871-877.
- 440 [13] Shanbara, H.K., Ruddock, F., and Atherton, W., *Rutting Prediction of a Reinforced Cold*  
441 *Bituminous Emulsion Mixture Using Finite Element Modelling.* Procedia Engineering, 2016. **164**:  
442 p. 222-229.
- 443 [14] Arabani, M., Jamshidi, R., and Sadeghnejad, M., *Using of 2D finite element modeling to predict*  
444 *the glasphalt mixture rutting behavior.* Construction and Building Materials, 2014. **68**: p. 183-191.
- 445 [15] Fang, H., et al., *On the characterization of flexible pavement rutting using creep model-based finite*  
446 *element analysis.* Finite Elements in Analysis and Design, 2004. **41**(1): p. 49-73.
- 447 [16] Chazallon, C., et al., *Modelling of rutting of two flexible pavements with the shakedown theory and*  
448 *the finite element method.* Computers and Geotechnics, 2009. **36**(5): p. 798-809.
- 449 [17] Kandhal, S. and Cooley, A., *EVALUATION OF PERMANENT DEFORMATION OF ASPHALT*  
450 *MIXTURES USING LOADED WHEEL TESTER.* 2002, National Center for Asphalt Technology:  
451 Auburn University, Alabama.
- 452 [18] Fernandes, F.M. and Pais, J.C., *Laboratory observation of cracks in road pavements with GPR.*  
453 Construction and Building Materials, 2017. **154**: p. 1130-1138.
- 454 [19] Franesqui, M.A., Yepes, J., and Garcia-Gonzalez, C., *Ultrasound data for laboratory calibration*  
455 *of an analytical model to calculate crack depth on asphalt pavements.* Data Brief, 2017. **13**: p.  
456 723-730.
- 457 [20] Chai, J.C. and Miura, N., *Traffic-Load-Induced Permanent Deformation of Road on Soft Subsoil.*  
458 JOURNAL OF GEOTECHNICAL AND GEOENVIRONMENTAL ENGINEERING, 2002.  
459 **128**(11): p. 907-916.

- 460 [21] Nik, A.A., Nejad, F.M., and Zakeri, H., *Hybrid PSO and GA approach for optimizing surveyed*  
461 *asphalt pavement inspection units in massive network*. Automation in Construction, 2016. **71**: p.  
462 325-345.
- 463 [22] Ambassa, Z., et al., *Fatigue life prediction of an asphalt pavement subjected to multiple axle*  
464 *loadings with viscoelastic FEM*. Construction and Building Materials, 2013. **43**: p. 443-452.
- 465 [23] Kim, H. and Buttlar, W.G., *Finite element cohesive fracture modeling of airport pavements at low*  
466 *temperatures*. Cold Regions Science and Technology, 2009. **57**: p. 123-130.
- 467 [24] Allou, F., et al., *Numerical finite element formulation of the 3D linear viscoelastic material model:*  
468 *Complex Poisson's ratio of bituminous mixtures*. Archives of Civil and Mechanical Engineering,  
469 2015. **15**(4): p. 1138-1148.
- 470 [25] Pérez, I., Medina, L., and del Val, M.A., *Nonlinear elasto-plastic performance prediction of*  
471 *materials stabilized with bitumen emulsion in rural road pavements*. Advances in Engineering  
472 Software, 2016. **91**: p. 69-79.
- 473 [26] Gu, F., et al., *Numerical modeling of geogrid-reinforced flexible pavement and corresponding*  
474 *validation using large-scale tank test*. Construction and Building Materials, 2016. **122**: p. 214-230.
- 475 [27] Huang, Y.H., *Pavement Analysis and Design*. 2004, United States of America: Pearson Education,  
476 Inc.
- 477 [28] Arabani, M. and Kamboozia, N., *The linear visco-elastic behaviour of glasphalt mixture under*  
478 *dynamic loading conditions*. Construction and Building Materials, 2013. **41**: p. 594-601.
- 479 [29] Shan, L., et al., *Optimization criterion of viscoelastic response model for asphalt binders*.  
480 Construction and Building Materials, 2016. **113**: p. 553-560.

- 481 [30] Zhang, J., et al., *Characterizing the three-stage rutting behavior of asphalt pavement with semi-*  
482 *rigid base by using UMAT in ABAQUS*. *Construction and Building Materials*, 2017. **140**: p. 496-  
483 507.
- 484 [31] European Committee for Standardization, *BS EN 933-1: Part 1, Tests for geometrical properties*  
485 *of aggregates: Determination of particle size distribution — Sieving method*, *British Standards*  
486 *Institution, London, UK, 2012*.
- 487 [32] European Committee for Standardization, *BS EN 12697-26: Part 26, Bituminous mixtures — Test*  
488 *methods for hot mix asphalt: Stiffness*, *British Standards Institution, London, UK, 2012*.
- 489 [33] European Committee for Standardization, *BS EN 12697-25: Part 25, Bituminous mixtures — Test*  
490 *methods for hot mix asphalt — Cyclic compression test*, *British Standards Institution, London, UK,*  
491 *2005*.
- 492 [34] Dulaimi, A., et al., *Laboratory Studies to Examine the Properties of a Novel Cold-Asphalt*  
493 *Concrete Binder Course Mixture Containing Binary Blended Cementitious Filler*. *Journal of*  
494 *Materials in Civil Engineering*, 2017. **29**(9).
- 495 [35] Dulaimi, A., et al., *Performance Analysis of a Cold Asphalt Concrete Binder Course Containing*  
496 *High-Calcium Fly Ash Utilizing Waste Material*. *Journal of Materials in Civil Engineering*, 2017.  
497 **29**(7).
- 498 [36] European Committee for Standardization, *BS EN 12697-22: Part 22, Bituminous mixtures — Test*  
499 *methods for hot mix asphalt — Wheel tracking*, *British Standards Institution, London, UK, 2003*.
- 500 [37] Xu, Q., Chen, H., and Prozzi, J.A., *Performance of fiber reinforced asphalt concrete under*  
501 *environmental temperature and water effects*. *Construction and Building Materials*, 2010. **24**(10):  
502 p. 2003-2010.

- 503 [38] Liu, G., Cheng, W., and Chen, L., *Investigating and optimizing the mix proportion of pumping*  
504 *wet-mix shotcrete with polypropylene fiber*. Construction and Building Materials, 2017. **150**: p.  
505 14-23.
- 506 [39] Jeon, J., et al., *Polyamide Fiber Reinforced Shotcrete for Tunnel Application*. Materials, 2016.  
507 **9**(3): p. 163.
- 508 [40] Hesami, S., Ahmadi, S., and Nematzadeh, M., *Effects of rice husk ash and fiber on mechanical*  
509 *properties of pervious concrete pavement*. Construction and Building Materials, 2014. **53**: p. 680-  
510 691.
- 511 [41] Gu, F., et al., *A mechanistic-empirical approach to quantify the influence of geogrid on the*  
512 *performance of flexible pavement structures*. Transportation Geotechnics, 2017. **13**: p. 69-80.
- 513 [42] Wu, J., Liang, J., and Adhikari, S., *Dynamic response of concrete pavement structure with asphalt*  
514 *isolating layer under moving loads*. Journal of Traffic and Transportation Engineering (English  
515 Edition), 2014. **1**(6): p. 439-447.
- 516 [43] Ghadimi, B., Nikraz, H., and Rosano, M., *Dynamic simulation of a flexible pavement layers*  
517 *considering shakedown effects and soil-asphalt interaction*. Transportation Geotechnics, 2016. **7**:  
518 p. 40-58.
- 519 [44] Souza, F.V. and Castro, L.S., *Effect of temperature on the mechanical response of thermo-*  
520 *viscoelastic asphalt pavements*. Construction and Building Materials, 2012. **30**: p. 574-582.
- 521 [45] Chun, S., et al., *Evaluation of interlayer bonding condition on structural response characteristics*  
522 *of asphalt pavement using finite element analysis and full-scale field tests*. Construction and  
523 Building Materials, 2015. **96**: p. 307-318.
- 524 [46] Kim, J., Lee, H.S., and Kim, N., *Determination of Shear and Bulk Moduli of Viscoelastic Solids*  
525 *from the Indirect Tension Creep Test*. journal of engineering Mechanics, 2010. **136**(9): p. 1067-  
526 1075.

- 527 [47] Li, Y., et al., *Effective temperature for predicting permanent deformation of asphalt pavement*.  
528 Construction and Building Materials, 2017. **156**: p. 871-879.
- 529 [48] Zhi, S., et al., *Evaluation of fatigue crack behavior in asphalt concrete pavements with different*  
530 *polymer modifiers*. Construction and Building Materials, 2012. **27**(1): p. 117-125.
- 531